Phases of phosphatidyl ethanolamine monolayers studied by synchrotron x-ray scattering

C. A. Helm,* P. Tippmann-Krayer,* H. Möhwald,* J. Als-Nielsen,‡ and K. Kjaer‡
*Department of Physical Chemistry, Johann Gutenberg University, D-6500 Mainz, West Germany; and ‡Physics Department, Risø National Laboratory, DK-4000 Roskilde, Denmark

ABSTRACT For the first time, phospholid monolayers at the air/water interface have been studied by x-ray diffraction and reflection all along the isotherm from the laterally isotropic fluid (the so-called LE phase) to the ordered phases. The model used to analyze the data, and the accuracy of the parameters deduced, were tested by comparing the results obtained with two lipids having the same head group but different chain lengths.

Compression of the fluid phase leads predominantly to a change of thickness of the hydrophobic moiety, much less of its density, with the head group extension remaining constant. The main transition involves a considerable increase (~10%) of the electron density in the hydrophobic region, a dehydration of the head group and a positional ordering of the aliphatic tails, albeit with low coherence lengths (~10 spacings). On further compression of the film, the ordered phase undergoes a continuous transition. This is characterized by an increase in positional ordering, a discontinuous decrease in lateral compressibility, a decrease in chain tilt angle with respect to the surface normal towards zero and probably also a head group dehydration and ordering.

INTRODUCTION

Phospholipid monolayers provide interesting model systems for the study of biological membranes because the monolayers enable investigations of interactions between lipids in well-defined arrangements while allowing a large degree of freedom in parameter variation. However, predominantly due to a lack of suitable experimental techniques, much remains to be learned about the molecular environment. Considerable progress has been achieved in this respect through the introduction of x-ray diffraction techniques for in situ studies of films at the air-water interface. Measurement of diffraction with in-plane scattering vector yields information on laterally periodic aliphatic chain arrangement within ordered lipid phases whereas reflectivity measurements with vertical scattering vector allow determination of the electron density along the surface normal regardless of any lateral ordering. Finally, so-called Bragg rod scans (with nonzero vertical and horizontal components of the scattering vector) provide vertical information about the diffracting part of the monolayer.

This work concerns two closely related monolayer systems at lateral pressures between 0 and 40 mN/m. It is demonstrated how the above-mentioned techniques can be used to derive microscopic information on condensed monolayer phases and on the phase transitions connecting them. The results are compared with those previously obtained for monolayers of other phospholipids and fatty acids.

SYSTEMS

Fig. 1 gives the surface pressure Π versus mean molecular area A for the lipids L-α-DiMyristoyl-Phosphatidyl-Ethanolamine (DMPE)[1] and L-α-DiLauroyl-Phosphatidyl-Ethanolamine (DLPE)[1]. DMPE distinguishes itself from other phospholipids by having the most pronounced changes in the isotherm slope at the pressures Π_c and Π_s (indicated in Fig. 1). On increase of the surface pressure Π above zero, an isotropic fluid phase (I)[2] appears. As Π exceeds Π_c, the Π vs. A isotherm becomes nearly horizontal, corresponding to the so-called main phase transition (first order) between the fluid and an ordered phase. In this regime (II), the two phases coexist (the names given here to regions I-III of the phase diagram will be justified below. Coexistence in region II of two phases of different densities has been observed in fluorescence micrographs of films on the water surface [Helm and Möhwald, 1988; Flörsheimer, 1989] and in electron micrographs of films transferred onto solid supports [Fischer and Sackmann, 1986]) and the area fraction of the ordered phase is increased on compression. The change of slope at Π_s has been observed as well in L-α-DiMyristoyl-Phosphatidic-Acid

[1] $(X\text{-}CH_2)\text{-}(X\text{-}CH)\text{-}CH_2\text{-}O\text{-}POOO^-\text{-}CH_2\text{-}CH_2\text{-}NH_3^+$, where X is $CH_3\text{-}(CH_2)_{12}\text{-}CO\text{-}O\text{-}$ for DMPE and X is $CH_3\text{-}(CH_2)_{10}\text{-}CO\text{-}O\text{-}$ for DLPE, see also Fig. 3.

(DMPA)[2] (Albrecht et al., 1978; Lösche, 1986; Lösche et al., 1984) and has been shown to be accompanied by an increase of positional ordering in the *solid* phase (III) for pressures $\Pi > \Pi_s$. (Kjaer et al., 1987; Helm et al., 1987*a*). The change of slope is typical of a second order phase transition. We note in passing that, on varying the temperature between 16°C and 39°C, Flörsheimer and Möhwald (1991) found no indication of a first order phase transition at Π_s.

A comparative study of DMPE and DLPE monolayers has the following advantages: the two molecules have identical head groups and hence, data obtained for this moiety can be checked for consistency.

Analogously, because the hydrophobic parts of the molecules differ by only two CH_2 groups per chain, consistency checks are possible for the chain parameters as well. Because the fluid phase of DLPE extends over a pressure range as large as 25 mN/m, the use of this lipid allows to study, e.g., density and hydration as functions of pressure in the fluid phase.

Further, it is to advantage that much data is already available for the two systems: thermodynamic and fluorescence microscopic data (Helm and Möhwald 1988; Flörsheimer, 1989) surface potential data (Miller et al., 1987), as well as electron diffraction and electron microscopy data on transferred films (Fischer and Sackmann, 1986).

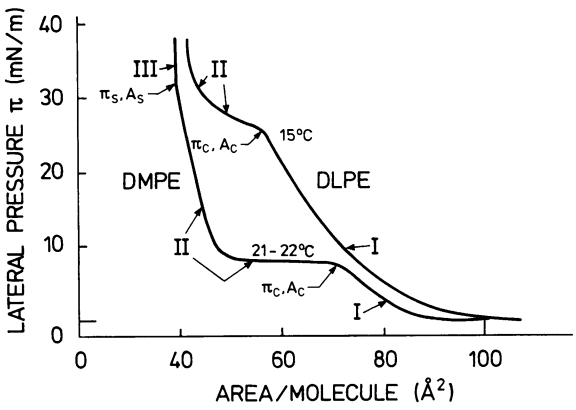

FIGURE 1 Pressure vs area isotherms for monolayers of DMPE at 21–22°C and DLPE at 15°C, corresponding to the x-ray experiments. Also indicated are the coordinates (A_c, Π_c) and (A_s, Π_s) of pronounced changes of slope of the isotherms as well as the corresponding regions (I, fluid phase; II, coexistence range; and III, solid phase).

EXPERIMENTAL

Langmuir troughs and monolayers

Dedicated Teflon™ Langmuir troughs (Gaines, 1966) measuring 80 × 135 × 13 mm^3 or 160 × 300 × 16 mm^3 were used for the x-ray experiments. The temperature was controlled by means of thermostated water flowing through the Teflon-clad metal bases of the troughs. The subphase temperature was constant to within ~0.5°C and we estimate the absolute accuracy of our thermometry to be better than ±2°C. Temperatures of 15°C (for the DLPE films) and 21–22°C (for DMPE films) were used.

The mean area per molecule, A, could be varied on line by moving the Teflon barrior manually or under computer control, and the resulting surface pressure, Π, was measured with a Wilhelmy balance (Gaines, 1966) which measures the differential pull on a partially submerged filter paper. The Wilhelmy balance was calibrated by means of the well known Π vs. A isotherm of Arachidic Acid (cf Albrecht et al., 1978). With time, drifts of the measuring system of up to 4 mN/m were experienced, as could be established by repeating the Π vs. A isotherms during an experiment. The singular points Π_c and Π_s of the isotherms (cf Fig. 1) remained clearly discernible, though, and thus the differential surface pressures Π–Π_c and Π–Π_s were measured with an error of <1 mN/m. Also, the purity and integrity of the films could be inferred from the shape of isotherms measured before, during and after the experiments. Trouble with achieving a quantitative deposition, as well as some loss of material from the monolayer during the experiments (due, perhaps, to leakage under the barrier) meant that the mean area per molecule, A, could not be inferred from the position of the barrier. Instead, it was deduced from the measured surface pressure Π or from the pressure differences Π–Π_s and Π–Π_c, by reference to standard isotherms measured (Helm and Möhwald, 1988; and Flörsheimer, 1989) on dedicated Langmuir troughs.

The lipids (chromatographically pure, from Sigma Chemical Company, St. Louis, MO) were dissolved in a 3:1 chloroform: methanol solution (analytic grade) and spread on Millipore™ filtered water (pH = 5.5).

X-ray equipment

The x-ray experiments were done at Hasylab, Desy, Hamburg, Germany with a synchrotron x-ray beam from bending magnet D of the electron storage ring Doris II which was operated at an energy of 3.7 GeV and currents of 20–100 mA.

At 20 m from the source, a Germanium (111) perfect

[2] (X-CH_2)-(X-CH)-CH_2-O-POOO$^-$, where X is CH_3-$(CH_2)_{12}$-CO-O-.

monochromator crystal selects a wavelength $\lambda = 1.379$ Å. By tilting the monochromator around a horizontal axis, the monochromatic beam can be deflected an angle α_i down onto the sample surface. The foot print of the beam on the sample surface is controlled by a slit 2 mm wide by 50–100 μm high in front of the sample and variations in the incident flux are monitored by means of a plastic foil which, mounted after the slit, scatters a small fraction of the beam into a NaI(Tl) scintillation x-ray counter. The Langmuir trough, enclosed in a gas-tight cannister with x-ray transparent windows, was mounted on a rotation stage and an elevator, allowing the sample to track the beam. A polished glass block, submerged in the trough underneath the x-irradiated area, reduced the water height to ~300 μm, thus effectively damping any mechanically excited waves on the water surface (cf Braslau et al., 1988; and Braslau et al., 1985).

X-ray optics at grazing incidence

By standard optics, x-rays incident on the horizontal air-water interface at a vertical angle α_i will be *reflected* at the angle $\alpha_f = \alpha_i \equiv \alpha$ (cf Fig. 2 *a*) and *transmitted* through the interface at the refracted angle α_i' (Als-Nielsen and Möhwald, 1989; Als-Nielsen and Kjaer, 1989; and Als-Nielsen, 1987), where

$$\alpha_i' = \sqrt{\alpha_i^2 - \alpha_c^2}. \tag{1}$$

Here, α_c is the critical angle for total external reflection, $\alpha_c = 0.0024$ rad $= 0.14°$ for water at the wave length used.

For a sharp, planar interface the reflectivity is given by Fresnel's law,

$$R_F = \left|\frac{\alpha - \alpha'}{\alpha + \alpha'}\right|^2 \rightarrow \left(\frac{\alpha_c}{2\alpha}\right)^4 \text{ for } \alpha \gg \alpha_c. \tag{2}$$

For $\alpha_i < \alpha_c$ the reflection is total, and below the interface, an evanescent wave travels parallel to the interface. Its intensity dies out exponentially in a penetration depth Λ below the interface. Λ is of order ~100 Å (e.g., Als-Nielsen and Kjaer, 1989). The transmitted intensity below the interface is given by

$$T_F = \begin{cases} |2\alpha/\alpha_c|^2, & 0 < \alpha < \alpha_c \\ \left|\dfrac{2\alpha}{\alpha + \alpha'}\right|^2, & \alpha > \alpha_c \end{cases} \tag{2a}$$

The above discussion ignores absorption of x-rays. Absorption, however, leads only to quantitatively very minor changes to the above description (e.g., Als-Nielsen and Kjaer, 1989).

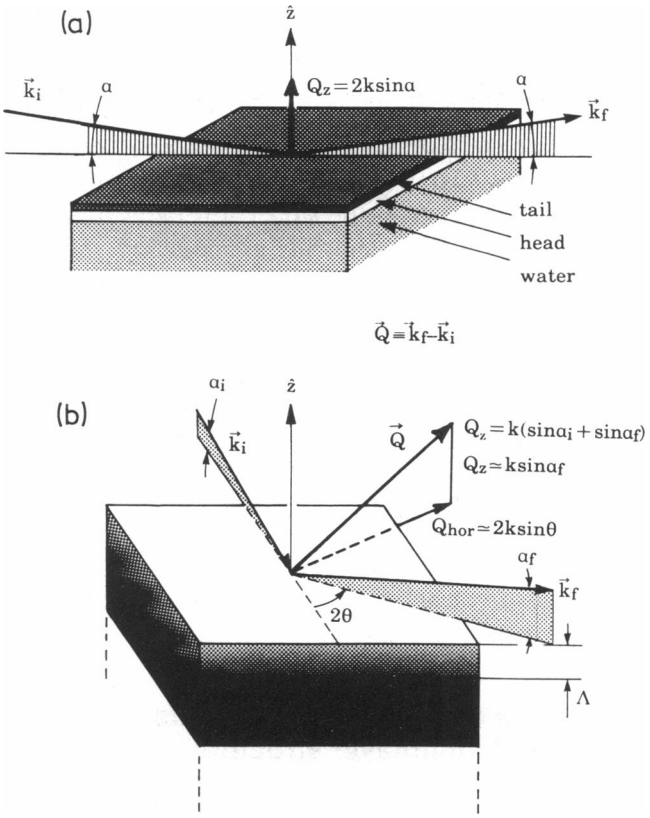

FIGURE 2 The scattering geometry. (*a*) X-ray specular reflectivity with vertical scattering vector $Q = (0, 0, Q_z)$ probes the vertical interfacial structure; and (*b*) x-ray diffraction with larger horizontal (Q_{hor}) than vertical (Q_z) scattering vector components. See text.

X-reflectivity experiments and vertical monolayer structure

To gain information about the vertical structure of the monolayer, vertical scattering is required, i.e., measurement of the x-ray specular reflectivity of the horizontal interface. To this end, the diffractometer is set for equal vertical incidence and exit angles, $\alpha_i = \alpha_f = \alpha$, and the horizontal scattering angle $2\theta = 0$ (Fig. 2 *a*). A 3 mm wide by 1 mm high slit in front of the NaI(Tl) detector serves to define the reflected beam. This geometry gives a purely vertical scattering vector,

$$\mathbf{Q} \equiv \mathbf{k}_f - \mathbf{k}_i, \tag{3}$$

$$\mathbf{Q} = (0, 0, Q_z), \quad Q_z = 2k \cdot \sin\alpha = \frac{4\pi}{\lambda} \cdot \sin\alpha, \tag{4}$$

where the final and initial wave vectors are $\mathbf{k}_f$, $\mathbf{k}_i$; $|\mathbf{k}_f| = |\mathbf{k}_i| = k = 2\pi/\lambda$. Eq. 4 ignores refraction effects (cf Eq. 2). This is a satisfactory approximation for $\alpha > 2 \cdot \alpha_c$, (Als-Nielsen and Kjaer, 1989). It is convenient to mea-

sure Q_z either in $Å^{-1}$ units or in units of the scattering vector Q_c corresponding to the critical angle:

$$Q_c \equiv 2 \cdot k \cdot \sin \alpha_c = 0.02176\ Å^{-1} \text{ for water.} \quad (5)$$

The experimentally accessed range was $0 < \alpha < 4.1°$ corresponding to $0 < Q_z < 0.65\ Å^{-1} \simeq 30 \cdot Q_c$.

The absolute reflectivity, $R(Q_z)$, was derived by normalization to the incident flux as measured with the sample lowered out of the beam. Also, the background, independently measured by displacing the detector and slit horizontally, was subtracted. The high intensities of the incident beam and of the reflected beam at lower angles were measured by means of a construction similar to that described above for the incident flux monitor. Then, at higher angles where the reflected signal is weak enough to be detected by the NaI detector directly, the relative efficiencies of the two detector configurations were determined experimentally, thus enabling continous measurement of $R(Q_z)$ over the required 10^8 dynamic range.

Horizontal diffraction experiments and lateral monolayer structure

The lateral structure of the monolayer is probed by horizontal diffraction (Fig. 2 b). The horizontal direction, 2θ, of the scattered photons was analyzed by means of a Soller collimator. Two Sollers giving 2θ resolutions of 0.08° or 0.15° full width at half maximum (FWHM), respectively, were employed.

Then, the horizontal and vertical components of the scattering vector **Q** are

$$Q_{hor} = k \cdot \sqrt{\cos^2 \alpha_i' + \cos^2 \alpha_f' - 2 \cos \alpha_i' \cdot \cos \alpha_f' \cdot \cos 2\theta}, \quad (6)$$

$$Q_z = k \cdot (\sin \alpha_i' + \sin \alpha_f'), \quad (7)$$

cf Fig. 2 *b*. Eqs. 6 and 7 contain the refraction-corrected incidence and exit angles α_i' and α_f' (cf Eq. 1). However, to reduce the background of photons scattered from the subphase, the incidence angle α_i was set below the critical angle α_c for total external reflection: $\alpha_i = 0.85 \cdot \alpha_c$. This limits the penetration ($1/e$ depth of the x-ray intensity) to $\Lambda = 87$ Å (Als-Nielsen and Möhwald, 1989, Eq. A3.12) and means that $\alpha_i' = 0$. (Thus, the 'incident' wave field to be diffracted by any in-plane structure is the above-mentioned evanescent wave which travels parallel to the interface). Also, α_f is a small angle, but somewhat larger than α_c, so that Eqs. 6 and 7 simplify to

$$Q_{hor} \simeq 2k \cdot \sin \frac{2\theta}{2} (+O(\alpha_f^2)), \quad (8)$$

$$Q_z \simeq k \cdot \sin \alpha_f. \quad (9)$$

Concerning α_f, for intensity reasons, in most of the experiments reported (cf Fig. 5 and 6 below) a finite vertical aperture was used, so that the detector integrated over a range $0 < \alpha_f < \alpha_{f,max} = 3.0°$ or 4.1° corresponding to $0 < Q_z < Q_{z,max} \simeq k \cdot \sin \alpha_{f,max} = 0.24$ or $0.33\ Å^{-1}$.

At the expense of a lower counting rate, more can be learned about the vertical variation of the horizontally diffracting part of the monolayer by simultaneously resolving the vertical (α_f) and horizontal (2θ) directions of the scattered rays. In a separate experiment (Fig. 7) a narrower vertical aperture, placed after the horizontally analyzing Soller collimator, gave resolutions FWHM (α_f) = 0.23° corresponding to FWHM(Q_z) = $0.019 Å^{-1}$ whereas α_f (or Q_z) was varied in the range 0 to 5.4° (or $0.43\ Å^{-1}$).

ANALYSIS

The scattered x-ray intensity is proportional to the Fourier-transform squared of the electron density $\rho(x, y, z)$ in the scatterer:

$$I(\mathbf{Q}) \propto |\int \rho(\mathbf{r}) e^{i\mathbf{Q} \cdot \mathbf{r}} d^3\mathbf{r}|^2. \quad (10)$$

It is convenient to separately consider the consequences of Eq. 10 for horizontal and for vertical scattering.

Analysis of horizontal x-ray scattering

For a monolayer with a laterally periodic (or quasiperiodic) structure, Eq. 10 leads to Bragg peaks at points

$$\mathbf{Q}_{hor} = \mathbf{G}_{h,k}, \quad (11)$$

of the two-dimensional reciprocal lattice (cf Als-Nielsen and Kjaer, 1989). Here, (h, k) are the familiar Miller indices. Notice that Eq. 11 constrains only the horizontal component of the scattering vector: the scattering is confined to so-called Bragg rods in reciprocal space (**Q**-space). Thus, at Bragg setting (Eq. 11) one can measure, as a function of the vertical scattering vector component Q_z, the Bragg intensity,

$$I_{hk}(Q_z) \propto A_{tot} \cdot \frac{1}{A_c^2} \cdot |F_p(\mathbf{G}_{hk}; Q_z)|^2 \cdot LP, \quad (12)$$

where A_{tot} is the total illuminated area contributing to the scattering, A_c is the lateral unit cell area (it will be apparent from the results reported below that the basic building block for a laterally periodic structure in DMPE monolayers is one hydrocarbon tail; thus, A_c is the area per tail, not per molecule) $LP = \cos^2(2\theta)/\sin(2\theta)$

is the Lorentz-polarisation factor and $F_p(\mathbf{Q})$ is the unit cell structure factor of the (quasi-) periodic part, $\rho_p(x, y, z)$, of the monolayer:

$$F_p(\mathbf{Q}) = \int_{z=-\infty}^{\infty} \int_{x,y \in A_c} \rho_p(x, y, z) \cdot e^{i\mathbf{Q}\cdot\mathbf{r}} dx\, dy\, dz. \quad (13)$$

Thus, information about the vertical ($z-$) variation of the diffracting (periodic) part of the monolayer can be obtained by resolving the Q_z-dependence of the Bragg scattering.

The nonperiodic part, $[\rho(x, y, z) - \rho_p(x, y, z)]$, of the interfacial density leads, for mainly horizontal scattering vector, to a diffuse scattering which cannot be separated from the background.

Bragg setting merely involves adjustment of the horizontal and vertical scattering angles 2θ and α_f, because the monolayer consists of randomly oriented domains.

Then, the d-spacing d_{hk} is given by Bragg's law,

$$d_{hk} = 2\pi/G_{hk} = \lambda/(2 \sin \theta) \quad (14)$$

and the measured line width FWHM(2θ), corrected for resolution effects, is related to the positional correlation length ξ by

$$\xi = \frac{2}{\mathrm{FWHM}(Q_{hor})} = \frac{\lambda}{\pi \cdot \cos\theta \cdot \mathrm{FWHM}(2\theta)}. \quad (15)$$

Analysis of x-ray reflectivity data

For the case of vertical scattering, $\mathbf{Q} = (0, 0, Q_z)$, Eq. 10 leads, after a partial integration, to the expression (cf Als-Nielsen and Kjaer, 1989),

$$R(Q_z) = R_F(Q_z) \cdot \left| \frac{1}{\rho_w} \int \frac{d\rho(z)}{dz} \cdot e^{iQ_z z} \right|^2 \quad (16)$$

$$= R_F(Q_z) \cdot \left| \frac{iQ_z}{\rho_w} \int \rho(z) \cdot e^{iQ_z z} \right|^2, \quad (17)$$

for the reflectivity $R(Q_z)$. Eqs. 16 and 17 ignores refraction and other "dynamical scattering" effects and is an adequate approximation for $Q_z > 2 \cdot Q_c$ (op. cit.) In Eqs. 16–17, $\rho(z)$ is the total electron density, whether periodic or not, laterally averaged over the coherence area of the x-ray beam (as discussed further below in detail), and ρ_w is the mean electron density of the water sub-phase, used also when calculating the 'Fresnel' reflectivity $R_F(Q_z)$.

To analyse the data, we have parametrised the vertical density $\rho(z)$ by describing it by regions ('boxes') of constant density (cf Fig. 3): one box for the tail section (density ρ_T; vertical extent ℓ_T), one for the head-group region (ρ_H; ℓ_H) and constant densities 0 and ρ_w in the air and subphase, respectively. This box model is then smeared by convolution with a Gaussian, $\exp(-\Delta z^2/2\sigma^2)$, which describes the experimentally observed diffuseness of the interfaces. The source of this diffuseness or roughness is mainly thermally excited capillary waves at the surface (cf Braslau et al., 1985; Braslau et al., 1988; Als-Nielsen and Möhwald, 1989; Als-Nielsen and Kjaer, 1989; Als-Nielsen, 1987; Kjaer et al., 1989; and Helm et al. 1987b). It leads to a Debye-Waller factor, $\exp(-Q_z^2\sigma^2)$, in the normalized reflectivity $R(Q_z)/R_F(Q_z)$.

Extracting for clarity the Debye-Waller factors, it is instructive to compare the formulas for reflectivity (Eq. 17):

$$R(Q_z)/R_F(Q_z) = e^{-Q_z^2\sigma^2} \cdot \left| 1 + \frac{iQ_z}{\rho_w \cdot A_c} F_{tot}(0, 0, Q_z) \right|^2, \quad (18)$$

and for horizontal diffraction (Eq. 12):

$$I_{hk}(Q_z) \propto e^{-G_{hk}^2\sigma_{hor}^2} \cdot e^{-Q_z^2\sigma_z^2} \cdot \left| \frac{F_p(\mathbf{G}_{hk}; Q_z)}{A_c} \right|^2. \quad (19)$$

The reflectivity probes the total interfacial structure (whether laterally periodic or not) and it contains interference between the subphase ("1" in Eq. 18) and the monolayer ("F_{tot}" in Eq. 18). By contrast, horizontal diffraction filters out the laterally (quasi-) periodic part of the interface and, in consequence, contains no contribution from the sub phase.

Next, we discuss in detail the various parameters of the box models (cf Fig. 3) used for analysing reflectivity data for the two monolayer phases. In the solid phase the hydrocarbon tails are vertically oriented and densely packed. The thickness, l_T, of the hydrocarbon layer is then expected (Kjaer et al., 1989; Als-Nielsen and Kjaer, 1989) to be

$$l_T = (12 + \%) \cdot 1.265\ \text{Å} = 16.6\ \text{Å for DMPE, and} \quad (20)$$

$$l_T = (10 + \%) \cdot 1.265\ \text{Å} = 14.1\ \text{Å for DLPE.} \quad (21)$$

In the most compressed state, the area per molecule is

$$A_s = 40\ \text{Å}^2, \quad (22)$$

and the tail density,

$$\rho_T = 2 \cdot 8/1.265\text{Å}/40\ \text{Å}^2 = 0.3162\, e/\text{Å}^3 = 0.946 \cdot \rho_w \quad (23)$$

A priori values of the head group layer thickness l_H and electron density ρ_H are more difficult to arrive at. One uncertainty is that the position of the interface between the tail and the head group layer can be determined only within limits. For the sake of simplicity, all hydrocarbon groups were assumed to belong to the tail layer. Then it

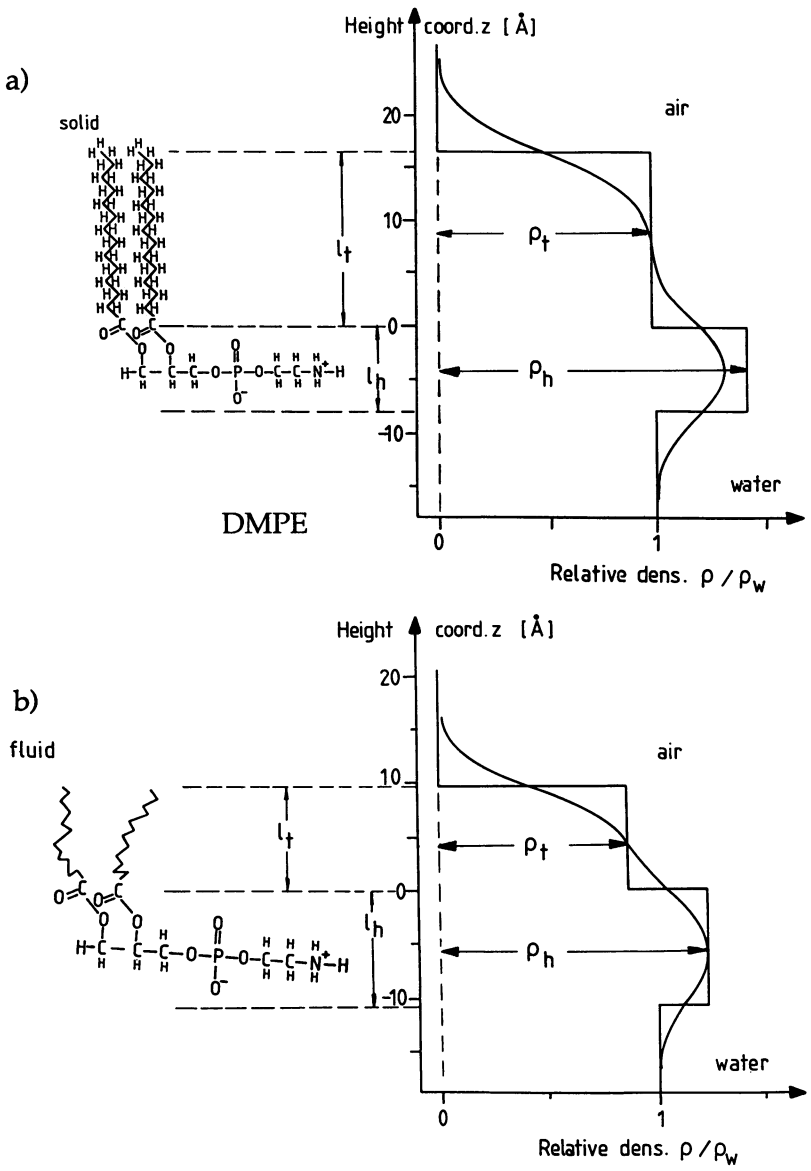

FIGURE 3 Sketch of the molecular arrangement and the corresponding electron density model distribution for (*a*) the solid and (*b*) fluid phases. Also shown are the definitions of the density model parameters: Layer thicknesses l_H, l_T, electron densities ρ_H, ρ_T, and the Gaussian smearing parameter σ.

is easy to obtain the number of electrons in the tail

$$N_T = 2 \times (12 \times 8 + 9) = 210 \quad \text{for DMPE, and}$$
$$N_T = 2 \times (10 \times 8 + 9) = 178 \quad \text{for DLPE.}$$

For consistency, in all fits of reflectivity curves the tail parameters were constrained to produce the same number of electrons in the tail, i.e.,

$$N_T = \rho_T \times l_T \times A = \text{constant.}$$

where A is the molecular area as obtained from the isotherms. How this assumption affects the analysis will be discussed in the discussion section.

The carbonyl and the phosphate groups contribute high electron densities, whereas the density of the ethanolamine group is close to that of water. Hence, this group cannot be distinguished from the surrounding water. Indeed, the head group layer incorporates both the lipid head group and any interpenetrating water

molecules. Thus, analysis of the data will yield information of hydration.

In the fluid phase (I) (lower part of Fig. 3) the area per molecule is increased, resulting in a smaller density of the electron rich head group layer. This effect is only in part compensated by increased hydration and thus ρ_H is expected to be smaller than for the solid phase. The hydrocarbon tails may take advantage of the increased area per molecule by an increase in the number of gauche defects or by tilting away from a vertical mean orientation (or both). In the former case both the density ρ_T and the thickness l_T will be reduced, whereas in the latter only case the layer thickness l_T will be reduced.

Reflectivity data for the coexistence region (II) could not be meaningfully analyzed by simultaneously fitting the parameters for the fluid and the solid component because the total number of fitted parameters becomes too large. However, if it is assumed that the coexisting phases have parameters identical to those obtained in the homogeneous regions (I) and (III) of Fig. 1, the data can be analyzed in terms of a superposition of the models arrived at for regions (I) and (III). Then, the only adjustable parameter is the area fraction Φ' of the solid phase. Two different ways of performing the superposition must be considered. (*a*) Incoherent superposition: if typical dimensions of the homogeneous domains of the coexisting phases are larger than the lateral coherence length of the Synchrotron x-ray experiment then the reflectivities, R_{fl} and R_s, of the two phases must be combined in proportion to the area fraction of each phase,

$$R = \Phi' \cdot R_s + (1 - \Phi') \cdot R_{fl}, \tag{24}$$

i.e.,

$$R/R_F = \Phi' \cdot \left| \frac{1}{\rho_w} \int dz\, \rho_s(z) e^{iQ_z \cdot z} \right|^2 + (1 - \Phi') \cdot \left| \frac{1}{\rho_w} \int dz\, \rho_{fl}(z) e^{iQ_z \cdot z} \right|^2; \tag{25}$$

(*b*) Coherent superposition: if the scale of lateral film inhomogeneities is smaller than the lateral coherence length of the Synchrotron x-ray experiment then one measures an average electron density $\rho(z)$ for the two phases, where

$$\rho(z) = \Phi' \cdot \rho_s(z) + (1 - \Phi') \cdot \rho_{fl}(z), \tag{26}$$

i.e.,

$$R/R_F = \left| \frac{1}{\rho_w} \int dz [\Phi' \cdot \rho_s(z) + (1 - \Phi') \cdot \rho_{fl}(z)] \cdot e^{iQ_z \cdot z} \right|^2. \tag{27}$$

Fig. 4 *a* shows the result of incoherent superposition (Eq. 25) for various Φ', assuming typical values for the solid ($\Phi' = 1$) and the fluid ($\Phi' = 0$) phase of DMPE. Of course, all curves intersect at the three points where the ($\Phi' = 0$) and ($\Phi' = 1$) curves intersect (the so-called isosbestic points of the family of curves). The insert (*c*) plots the scattering vector Q_{min} (corresponding to the minimum of R/R_F) vs. the molar fraction Φ of the solid phase (cf Eqs. 41 and 42). It appears that Q_{min} depends almost linearly on Φ. Fig. 4 *b* shows the result of coherent superposition (Eq. 27), using the same parameter values as above. One isosbestic point is gone (and the remaining two are fortuitous).

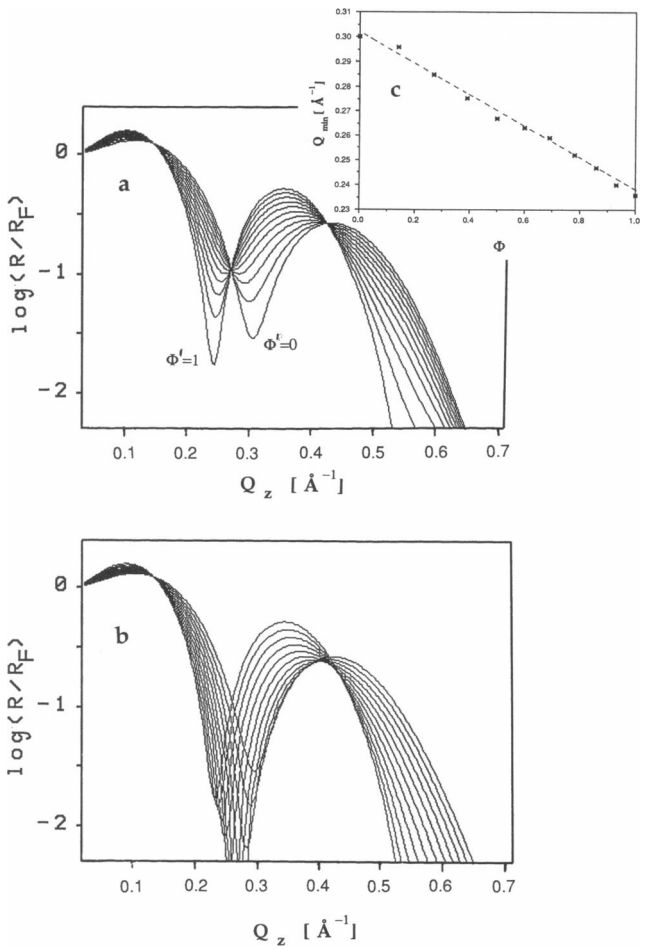

FIGURE 4 Calculated normalized reflectivity R/R_F vs vertical scattering vector Q_z for the phase coexistence range, for the case of (*a*) incoherent and (*b*) coherent superposition. Φ', varied in steps of 0.1, denotes the area fraction of the solid phase. The insert shows the minimum position Q_{min} as a function of the molar fraction Φ for incoherent superposition. Parameters for the coexisting phases (corresponding to $\Phi = \Phi' = 0$ and $\Phi = \Phi' = 1$) were those actually fitted to the DMPE data (Fig. 8, *m* and *c*).

Fluorescence microscopy measurements show that the solid domains are several tens of micrometers large (Helm and Möhwald, 1988; Flörsheimer, 1989) (i.e., somewhat larger than the experimental lateral coherence length of $\leqq$10,000 Å) and therefore, incoherent superposition (Eq. 25) applies. The experimental results given below are consistent with Eq. 25.

EXPERIMENTAL RESULTS AND INTERPRETATION

In-plane diffraction, integrated over Q_z

Because scans which resolve both Q_{hor} and Q_z have low counting rates and require many points, most of the in-plane diffraction was done in a mode which integrates over Q_z (cf section on horizontal diffraction experiments and lateral monolayer structure). Typical scans are shown in Fig. 5 (*a–f*). At ~zero pressure (5 *a*) only a uniform background results. With decreasing area, a single broad, weak peak appears only when the pressure starts to rise above Π_c. On further compression, the peak shifts while becoming sharper and more intense. The full lines are Lorentzian line shapes, convoluted with the measured experimental resolution (Fig. 5 *g*). We also tried fitting the data with a Gaussian line shape. At the lower pressures, when the peaks are weak and broad, equally good fits resulted, but for $\Pi >$ ~20 mN/m, when the peaks sharpen up and become more intense, the Lorentzian profile gave significantly better fits. Fig. 6 shows parameters extracted from diffraction groups (including those of Fig. 5) as functions of the mean area per molecule A (Fig. 6 *a*) and of the pressure difference Π–Π_s (Fig. 6 *b*). First we consider the peak position Q_{hor} or the corresponding spacing $d = 2\pi/Q_{hor}$ (*bottom panels*). Fig. 6 *b* shows the d-spacing from two different films. A difference of ~0.01 Å is apparent. This difference is outside experimental error but we cannot explain its reason. One possibility is trapping of physical or chemical impurities, or ageing, but no systematic studies of this effect have been performed.

With increasing Π, one observes an approximately linear decrease of d, with two different slopes for $\Pi < \Pi_s$ and $\Pi > \Pi_s$. The area compressibility κ_d determined from the lattice spacing d of a hexagonal lattice is given by

$$\kappa_d = -\frac{2}{d} \cdot \frac{d(d)}{d\Pi} . \qquad (28)$$

Because d varies little, the linear slopes in Fig. 6 *b* yield a constant compressibility in the two regions $>(\kappa_d = 0.79$ or $0.5 \cdot 10^{-3}$ m/mN for the the two films) and $<\Pi_s$ ($\kappa_d = 1.6 \cdot 10^{-3}$ m/mN) respectively. The discontinuity of κ_d at Π_s without any cusp or divergence at Π_s then indicates a second order phase transition.

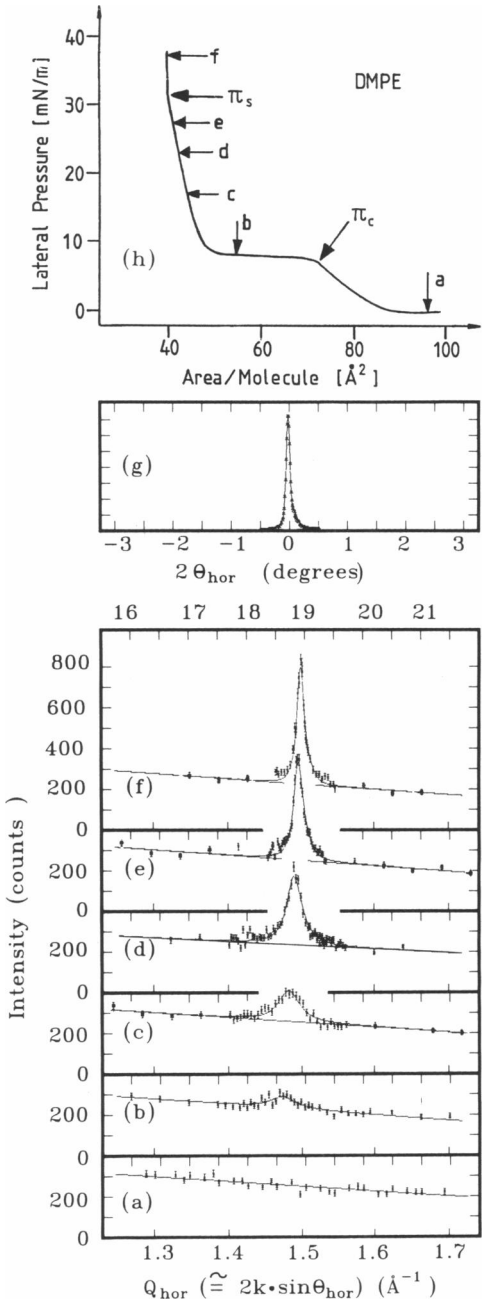

FIGURE 5 In-plane diffraction data (intensity [integrated over $Q_z = 0$ to 0.33 Å^{-1}, cf text] vs Q_{hor} or vs 2θ) from a monolayer of DMPE for increasing pressure (*a–f*). The full lines are fitted Lorentzian profiles, $1/(1 + \xi^2 \cdot [Q - Q_{peak}]^2)$ convoluted with the experimental resolution function, which is shown in panel (*g*). Panel (*h*) gives the (A, Π) values for the diffraction groups (*a*)–(*f*).

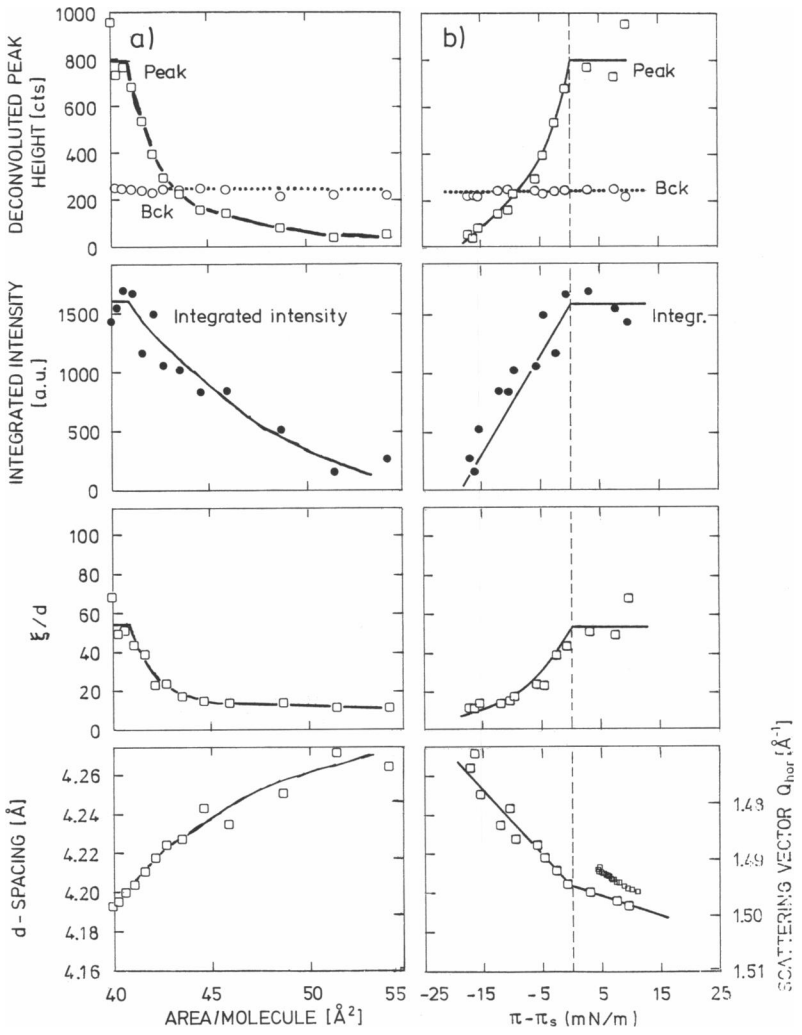

FIGURE 6 (*a*) Parameters extracted from the DMPE diffraction data [deconvoluted peak height, background level, integrated intensity, ξ/d, the positional correlation range in units of the lattice spacing, and the spacing d (left-hand scale) or peak position $Q_{hor} = 2\pi/d$ (right-hand scale)] vs mean molecular area A. (*b*) The same parameters as in (*a*), but plotted vs Π-Π_s. d-spacing data are shown for two different films. ([*Smaller squares*] Data from film No. 2, aged 1.5–9 h in the trough. The film was compressed to Π_s + 12 mN/m, then, with the barrier stationary, the peak was continuously remeasured as the pressure slowly relaxed to Π_s + 4 mN/m . [*Larger squares*] data from film No. 1, aged 35–51 h in the trough; Apart from one point, the data was taken on compression of the film.)

The value of κ_d should also be compared with

$$\kappa_A = -\frac{1}{A}\frac{dA}{d\Pi} \tag{29}$$

derived from the pressure area isotherm. For the steepest section of the isotherm $> \Pi_s$ one calculates a value of $\kappa_A = 1.4 \cdot 10^{-3}$ m/mN. This is about a factor of two $\times\kappa_d$ for $\Pi > \Pi_s$ and demonstrates that κ_A is to some extent determined by annealing of lattice defects and domain rearrangement, as was also found for DMPA monolayers. (Kjaer et al., 1987; Helm et al., 1987*a*).

The positional correlation length, ξ, increases continuously from 10–15 spacings at pressures just $> \Pi_c$ where the peak is first discernible with our set up to 50–70 spacings $> \Pi_s$. Concurrently, the integrated intensity increases ten-fold. The peak intensity is essentially the integrated intensity times the correlation length. The data of Fig. 6 are consistent with a second order phase transition at Π_s. Above Π_s, only the peak position continues to change; the intensity and the correlation length remain constant within the accuracy of the data.

Diffraction data with Q_z resolved:rod scans

One Bragg rod scan (cf section on horizontal diffraction experiments) was obtained for a monolayer of DMPE

compressed $> \Pi_s$. Fig. 7 shows the results. Fig. 7 *a* shows the diffracted intensity as a function of Q_{hor} and Q_z. On top of an approximately flat background, a sharp peak at $Q_{hor} \simeq 1.5$ Å^{-1} is apparent. As a function of Q_z the intensity extends to $\sim Q_z = 0.3$ Å^{-1}, whereas the Q_{hor} peak position remains constant. Also, the width in Q_{hor} does not depend on Q_z, as is apparent from Fig. 7 *b* which shows, as functions of Q_z, both the Q_{hor}-integrated intensities of the scans of Fig. 7 *a* (*squares*) and the intensity of a scan along Q_z with Q_{hor} at the peak position (*disks*). The two are indeed proportional. The curves are the results of model calculations to be described below. The dotted curve gives the calculated Bragg rod intensity profile $I_{|hk|}(Q_z)$ before correcting for the finite vertical experimental resolution. It is shown here for demonstration purposes only. The full curve is the same model, but convoluted with the experimental resolution. The full curve describes the data well.

Because it is the hydrocarbon tails ($[CH_2]_{12}CH_3$) which are the building blocks of the laterally periodic structure giving rise to the observed diffraction peaks, the model includes only the tails. Further, it describes them as being cylindrically symmetric and longitudinally uniform of length L (cf Als-Nielsen and Kjaer, 1989; Jacquemain et al., 1989; Jacquemain et al., 1990; Kjaer et al., 1989). This is an adequate description for the ranges of Q_{hor} and Q_z considered here, and it leads to the intensity of a Bragg rod (h, k) of a single domain being

$$I_{hk}(Q_z) \propto |V(x) \cdot F(\mathbf{G}_{hk}; Q_z)|^2 \cdot e^{-Q_z^2\sigma^2}, \tag{30}$$

with the structure factor

$$F(G_{hk}; Q_z) = F_{rad}(Q_{rad}) \cdot F_{long}(Q_{long}), \tag{31}$$

approximately factorized in a radial and a longitudinal part.

The corresponding components of the scattering vector Q are

$$Q_{rad} = \sqrt{Q_y^2 + (Q_x \cos t + Q_z \sin t)^2} \tag{32}$$

$$Q_{long} = Q_z \cos t - Q_x \sin t. \tag{33}$$

Eqs. 32–33 describe a uniform tilt (inclination angle t) of all the molecules in a horizontal direction $\hat{\mathbf{x}}$, so that

$$Q_x = |\mathbf{G}_{hk}| \cos \Psi_{hk}, \tag{34}$$

$$Q_y = |\mathbf{G}_{hk}| \sin \Psi_{hk}, \tag{35}$$

where Ψ_{hk} is the angle from $\hat{\mathbf{x}}$ to $\mathbf{G}_{hk}$. The variation of the radial from factor F_{rad} can be ignored for the **Q**-range used, and under the stated assumptions,

$$F_{long}(Q_{long}) = \frac{\sin \frac{1}{2} Q_{long} \cdot L}{\frac{1}{2} Q_{long} \cdot L}. \tag{36}$$

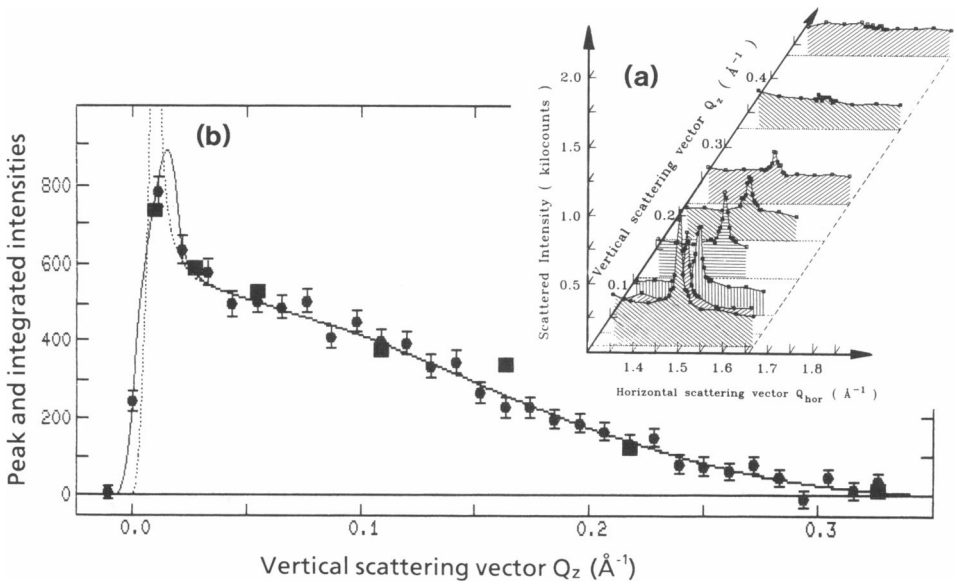

FIGURE 7 Bragg rod data for a compressed monolayer of DMPE. (*a*) Diffracted intensity vs horizontal scattering vector Q_{hor} and vs vertical scattering vector Q_z. (*b*) Rod intensity vs vertical scattering vector Q_z. *Squares:* Integrated intensity (in arbitrary units, back-ground subtracted) extracted from the scans in (*a*). *Disks:* Peak intensity (in counts, back-ground subtracted) from a Q_z scan along the Bragg rod at the optimum Q_{hor}. *Dotted curve:* Calculated intrinsic Bragg rod profile corresponding to the parameters discussed in the text. *Full curve:* Same, but convoluted with the experimental vertical resolution.

The Debye-Waller factor is exp $(-Q_z^2 \cdot \sigma^2)$, and the factor $V(x)$ (cf Vineyard, 1982) describes the interference between x-rays diffracted directly up into the Bragg rod and rays diffracted down and then reflected in the interface,

$$V(x) = \begin{cases} 2x & , \ 0 < x < 1 \\ \dfrac{2x}{x + \sqrt{x^2 - 1}} & , \ x > 1 \end{cases} , \tag{37}$$

$$x \equiv \alpha_f / \alpha_c = 2Q_z / Q_c. \tag{38}$$

($V^2(x)$ is analogous to the transmission factor T_F for the incident beam [Eq. 2 *a*]).

Finally, the total Bragg rod intensity profile

$$I_{|hk|}(Q_z) = \sum_{(h,k)} I_{hk}(Q_z), \tag{39}$$

results from adding the six equivalent lowest order reflections of the hexagonal crystal: $(h, k) = \pm(1, 0)$, $\pm(0, 1)$, and $\pm(1, -1)$. Results with other monolayers (Als-Nielsen and Kjaer, 1989; Jacquemain et al., 1989, 1990; Kjaer et al., 1989, Kenn et al., 1991; Leveiller et al., 1991) show that the Bragg rod intensity profile is quite sensitive to molecular tilt. This is because the molecular form factor (Eq. 36) is sharply peaked at $Q_{long} = 0$ which, according to Eqs. 33–34 means that for tilted molecules the (h, k) rod intensity will peak at a nonzero Q_z given by (op. cit.)

$$Q_{z,peak} \simeq \tan(t) \cdot G_{hk} \cdot \cos \Psi_{hk}. \tag{40}$$

The model, Eqs. 30–40, was least squares fitted to the data of Fig. 7 *b*, adjusting a scale factor, the length L of the diffracting tails, the molecular tilt-angle t and the roughness σ. The fittings give an upper bound of $\sim 5°$ on the tilt-angle t, and are compatible with $t = 0°$. For such small inclinations t, the horizontal direction, Ψ, of the tilt has little influence on the rod scan profile. For $t \simeq 0°$, L and σ are strongly correlated and cannot be independently fitted. The curves in Fig. 7 *b* were drawn with $L \equiv 16.6$ Å (Eq. 20), $t \equiv 0°$ and σ fitted to 1.5 ± 0.3 Å. An almost equally good fit results with $\sigma \equiv 3$ Å (as found in the x-ray reflectivity measurements, cf Table 1, next section), $t \equiv 0°$, and L fitted to 14.6 ± 0.3 Å. This value of L is, however, at variance with the length of the extended hydrocarbon tail (Eq. 20). A possible explanation is that the top end of the hydrocarbon tails are partially disordered and thus do not contribute to the Bragg rod. Molecular dynamics calculations (Bareman et al., 1988) on alkane monolayers seem to lend some credence to such a scenario.

It is also worth mentioning that in other Bragg rod studies of Langmuir films (op. cit.), a smaller roughness σ_{BR} was found than the roughness σ_{XR} deduced from reflectivity studies of the same systems (Kjaer et al., 1989, Wolf et al., 1988), even when the data allowed an independent determination of σ_{BR}. It is indeed conceivable that σ_{BR} might differ from σ_{XR}, because the effective roughness results from thermally excited capillary waves with wave vectors within a window determined by the experimental resolution (Braslau et al., 1985; Braslau et al., 1988; Daillant et al., 1989; Als-Nielsen and Kjaer, 1989) or, for the BR case, by the lateral positional correlation range (Kjaer and Als-Nielsen, unpublished). An in-depth discussion of this problem is, however, beyond the scope of this article.

In conclusion, the Bragg rod data indicate $t < 5°$, with $t = 0°$ the most probable value. The data are consistent with the expected value $L = 16.6$ Å (Eq. 20) and a roughness $\sigma_{BR} = 1.5$ Å, but other (correlated) values of L and σ_{BR} are possible.

Preliminary further rod scan measurements (Möhwald et al; 1990) indicate that at pressures $< \Pi_s$, the tails tilt uniformly in a direction between nearest neighbors. Further work on Bragg rods from DMPE and DSPE monolayers is in progress.

Reflectivity data

Fig. 8 shows the normalised x-ray reflectivity R/R_F vs. vertical scattering vector Q_z for a DMPE monolayer. The surface pressure increases from bottom to top of the figure. For clarity of presentation, the three different monolayer regimes are displayed in different ways. For the fluid phase (I), the data were fitted by the model described above and the best fits are shown as full lines. The data sets are displaced by one log unit (Fig. 8 *a*). With increasing Π, the minimum position Q_{min} shifts inwards, and the minimum becomes deeper, indicating an increase of the film thickness, and an increased density contrast between tail and head.

Data for the phase coexistence region (II) are superimposed in Fig. 8 *b*. For clarity the data are represented by smooth curves. As expected for coexistence between a solid and a fluid phase, the minimum position Q_{min} decreases monotonically with increasing pressure, cf Fig. 4, whereas the depth of the minimum behaves nonmonotonically. To a good approximation, all the curves *e–h* go through an isosbestic point at $Q_z \approx 12\, Q_c$, whereas the curves i, j, k are displaced from this point. A more detailed analysis using the incoherent superposition rule, Eqs. 24–25 and the lever rule, Eq. 42 below, gave unsatisfactory fits to the data, especially to those (i, j, k) at higher pressures. These observations indicate

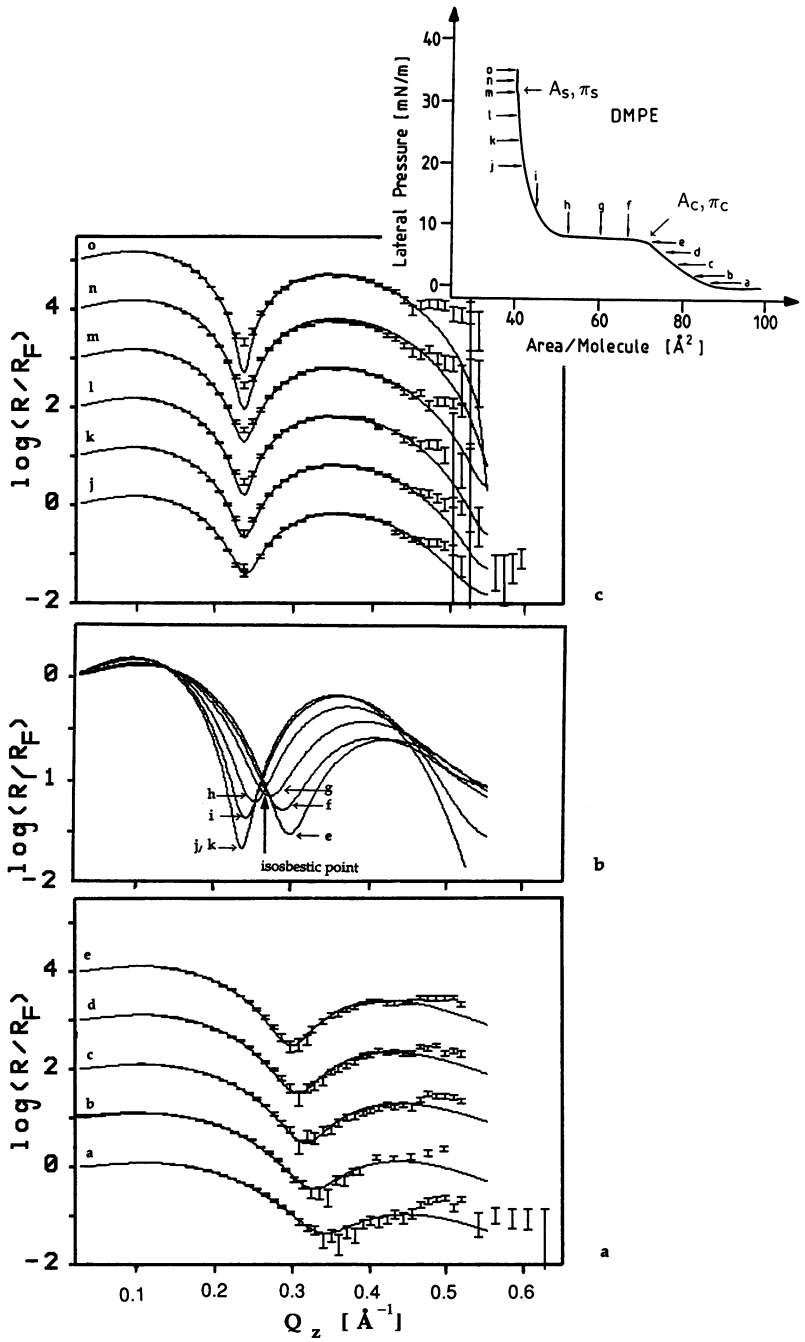

FIGURE 8 Normalized reflectivity R/R_F vs vertical scattering vector Q_z for DMPE monolayers. The insert gives the (A, Π) values for the data. Fig. 8 *a*, *a–e*: Fluid phase. Consecutive curves displaced one log unit. Full lines are fits of the two-box model with parameters given in Table I and Fig. 10. Fig. 8 *b*, *e–k*: Phase coexistence range. Full lines merely interpolate smoothly between the data points which were omitted for clarity. Fig. 8 *c*, *j–o*: Region near Π_s. Consecutive curves displaced one log unit. Full lines are fits of the two-box model with parameters given in Table I and Fig. 10.

that, especially at the higher pressures, at least one of the coexisting phases is modified.

Data for pressures approaching and exceeding Π_s are displayed in Fig. 8 *c*. The abscissae corresponding to the extrema are approximately constant on compression, whereas the height of the second maximum decreases slightly

Fig. 9 gives data for the fluid phase (Fig. 9 *a*) and the

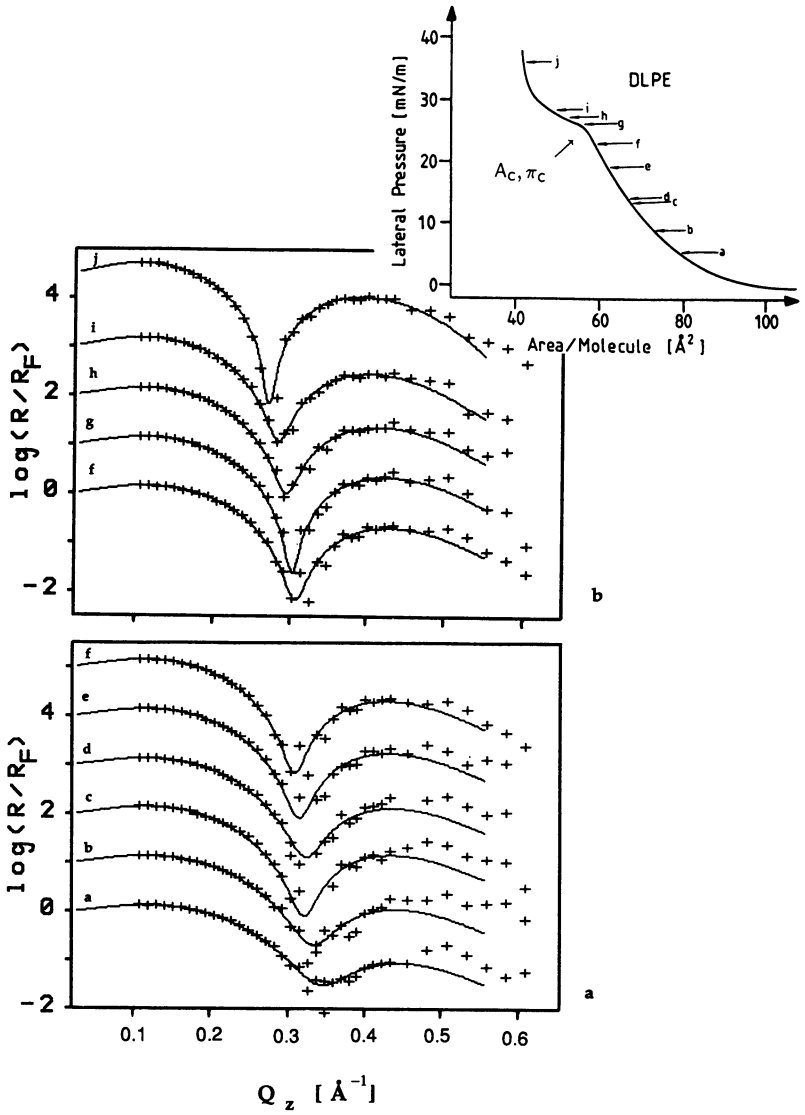

FIGURE 9 Normalized reflectivity R/R_F vs vertical scattering vector Q_z for DLPE monolayers. The insert gives the (A, Π) values for the data. Fig. 9 *a*, *a–f*: Fluid phase. Consecutive curves displaced one log unit. Full lines are fits of the two-box model with parameters given in Table 2 and Fig. 10. Fig. 9 *b*, *g–j*: Phase coexistence range. Consecutive curves displaced one log unit. Full lines are guides to the eye.

coexistence range (Fig. 9 *b*) of DLPE monolayers. Essentially the same features are observed as for DMPE, the differences being that a larger variation is seen for the fluid phase of DLPE, whereas a smaller variation than for DMPE is observed for the DLPE coexistence region. This can be qualitatively understood because the fluid (respectively the coexistence) regime extends over a larger (respectively smaller) range of average molecular area A in DLPE than in DMPE.

Due to the larger scatter of the data, less accurate conclusions are possible for the fluid phase of DLPE than for DMPE (compare Fig. 9 *a* and 8 *a*).

Fig. 10 shows the results of fits of two-box models (as described above) to the data obtained from single-phase or nearly-single-phase films of both DMPE and DLPE. For DMPE, a substantial amount of data is available around the phase transition point at $(A, \Pi) = (A_s, \Pi_s)$, $A_s \approx 40$ Å^2. No discontinuity in any of the parameters of Fig. 10 marks the transition point, indicating a second order transition.

The increase of the smearing parameter σ with decreasing molecular area will be discussed in a separate publication (Möhwald et al., unpublished data). Suffice to say that σ increases monotonically with increasing surface pressure Π (decreasing surface tension; decreasing area per molecule). The observations can be semi-

TABLE 1 **Results of fits of the two-box electron density model (cf Fig. 2) to x-ray reflectivity data for DMPE (cf Fig. 8)**

	A Å²	ρ_T/ρ_w —	ρ_H/ρ_w —	l_T Å	l_H Å	$l_T + l_H$ Å	N_T —	N_H —	σ Å
a	85.5	0.871	1.201	8.44	11.07	19.51	210	380	3.02
b	81.1	0.868	1.219	8.93	11.18	20.11	210	369	3.03
c	77.4	0.854	1.224	9.51	10.93	20.44	210	346	2.82
d	73.7	0.863	1.232	9.88	11.11	20.99	210	337	2.85
e	70.0	0.871	1.243	10.31	10.93	21.24	210	318	2.88
j	42.8	0.984	1.38	14.93	9.50	24.43	210	186	3.21
k	42.1	0.974	1.43	15.34	8.81	24.15	210	177	3.37
l	41.6	0.971	1.45	15.56	8.52	24.08	210	172	3.44
m	41.1	0.981	1.45	15.60	8.43	24.03	210	168	3.49
n	40.7	0.981	1.50	15.74	8.04	23.78	210	164	3.57
o	40.0	0.980	1.54	16.04	7.55	23.59	210	155	3.88
Formula:							210	140	

TABLE 2 **Results of fits of the two-box electron density model (cf Fig. 2) to x-ray reflectivity data for DLPE (cf Fig. 9)**

	A Å²	ρ_T/ρ_w —	ρ_H/ρ_w —	l_T Å	l_H Å	$l_T + l_H$ Å	N_T —	N_H —	σ Å
a	77.2	0.863	1.24	8.00	11.80	19.80	178	377	3.09
b	72.8	0.860	1.26	8.51	11.66	20.17	178	357	3.06
c	68.3	0.852	1.29	9.16	11.38	20.54	178	335	3.08
d	66.2	0.872	1.28	9.23	10.95	20.18	178	310	3.20
e	63.0	0.878	1.31	9.64	10.89	20.53	178	300	3.14
f	59.5	0.890	1.32	10.06	10.53	20.59	178	276	3.17
j	42.0	0.955	1.57	13.28	7.72	21.00	178	170	3.79
Formula:							178	140	

quantitatively explained if, as was found for a clean water surface (Braslau et al. 1988), the surface roughness σ can be described in terms of thermally excited capillary waves with a density of states described only by the reduced surface tension.

The data points for the two highest molecular areas for either lipid (Fig. 10) were obtained for lateral pressures close to zero where large surface inhomogeneities are observed due to coexistence between the isotropic fluid with a dilute gaseous phase. These data points will be disregarded in the discussion following below.

Fig. 11 gives the position $Q_z = Q_{min}$ of the first minimum of the normalized reflectivity R/R_F vs. molecular area A. As previously noted (Als-Nielsen and Kjaer, 1989), the inverse minimum coordinate Q_{min}^{-1} is an approximate measure of the film thickness:

$$l_T + \frac{1}{2} l_H \simeq \frac{3\pi/2}{Q_{min}}, \qquad (40a)$$

independent of the details of the model assumed, provided only that the tail layer has a density not too far from that of water whereas the head layer has a somewhat larger density. Note the linear dependence of Q_{min} on molecular area A for pressures $\Pi > \Pi_c$. For DMPE the linear law holds for areas A between 43 Å² and 68 Å², whereas for smaller areas Q_{min} is constant.

DISCUSSION

We start the discussion at low pressures and compare the two lipids as we go along the isotherm.

Fluid phase (l).

No in-plane diffraction peaks were observed in this phase, indicating positional correlation lengths ξ less than about five spacings and/or a vanishing small long-range order parameter.

With DLPE, this phase could be studied over a wide range of pressure and molecular area. Increasing the lateral pressure Π from 5 mN/m to 25 mN/m (decreasing A from 80 Å² to 57 Å²) causes the thickness l_T of the

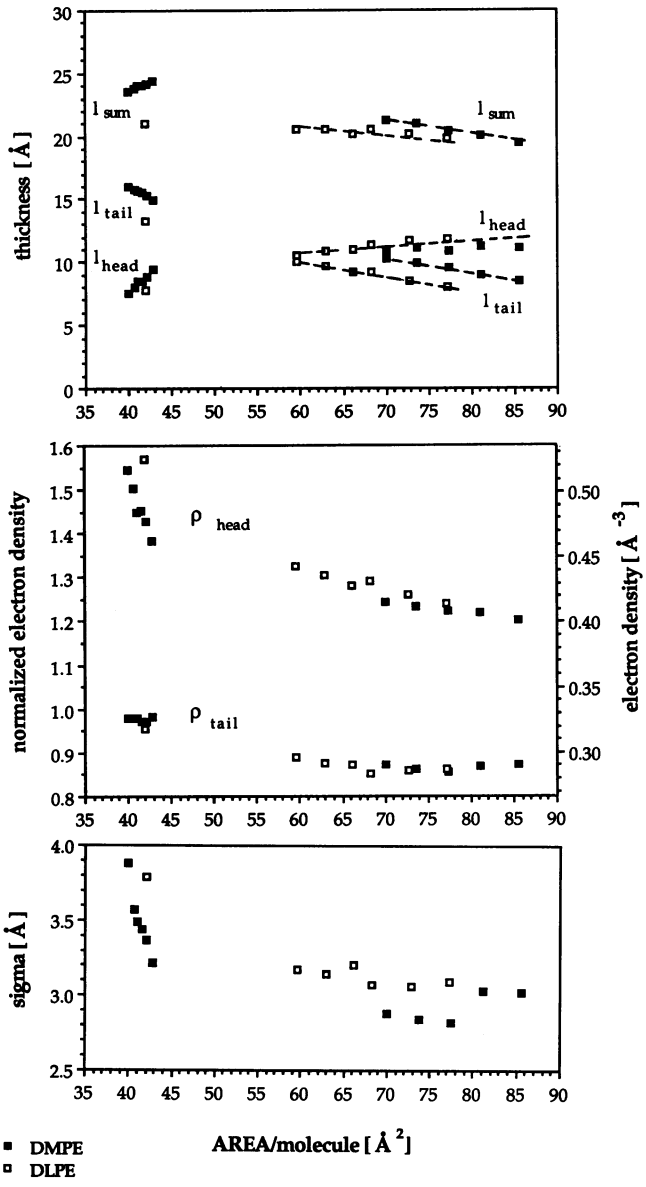

FIGURE 10 Structural parameters of monolayers of DMPE (*filled symbols*) and DLPE (*open symbols*), deduced from the reflectivity data of Figs. 8 and 9. The left part of the figure shows the region near Π_s and the right part shows the fluid phase. The parameters plotted vs mean molecular area A are: l_H, l_T and l_{sum}: thicknesses of head layer, tail layer and total film. ρ_H and ρ_T: electron densities of head and tail layer, normalized to the electron density of water (left-hand scale) and in units of electrons per Å^3 (right-hand scale). σ: Gaussian smearing parameter.

hydrocarbon tail layer to increase from ca. 8 Å to ~10 Å. This is as expected as film compression should bring about an average tail orientation closer to the vertical. Also, an increase of ~6% in the tail electron density results. Hence, a decrease of average molecular area of

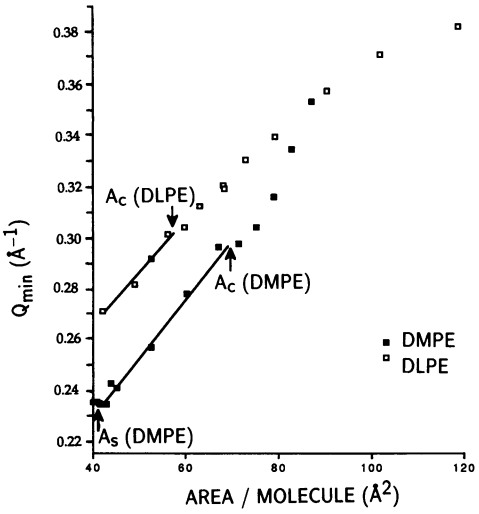

FIGURE 11 Position Q_{min} of the first minimum of the normalized reflectivity R/R_F of Figs. 8 and 9. Filled symbols for DMPE, open symbols for DLPE.

29% brings about an increase of l_T of 25% and an increase of ρ_T of 6% (from $0.84 \cdot \rho_w$ to $0.89 \cdot \rho_w$). For DMPE, qualitatively the same features are observed although for this lipid the variation within the fluid phase is less pronounced.

The results for the head group parameters obtained for DMPE and DLPE are mutually consistent. However, the values of l_H are larger than expected from Fig. 3,

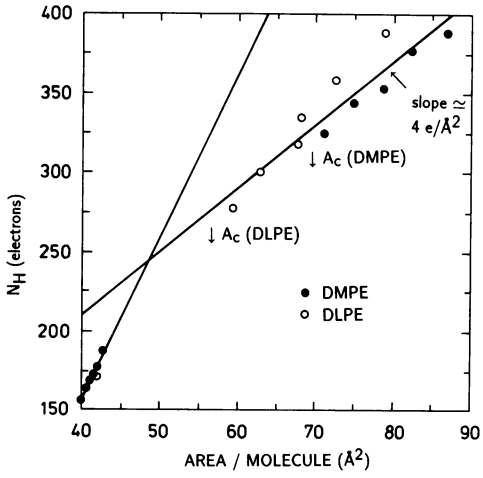

FIGURE 12 Number of electrons in the head group per lipid, $N_H = \rho_H \cdot l_H \cdot A$, vs mean molecular area A for monolayers of DMPE (*filled symbols*) and DLPE (*open symbols*) in the fluid phase and near Π_s. The straight lines were fitted to the values from both films for either regime.

according to which the head group extension l_H should not exceed 9 Å, the value obtained for the solid phase. This may indicate that the molecular model of Fig. 3 is too simple to account for the finer details of the atomic arrangement in the head group region. Indeed, according to the crystallographic study of Elder et al. (1977), in three-dimensional crystals, the two carbonyl groups of a phospholipid molecule are at different positions along the direction of the hydrocarbon chains. If this is the case for the monolayers (such structural details cannot necessarily be deduced for the monolayer by analogy with micro-emulsion or crystal structures since packing constraints involving neighbouring layers are absent in the case of monolayers) the head group layer thickness l_H would be extended at the expense of the tail section. This is in agreement with the findings of this study (see also the discussion below on the tail sections).

To obtain information about head group hydration we consider the number of electrons (per molecule) in the head group layer,

$$N_H = \rho_H \cdot l_H \cdot A,$$

where A is the molecular area. N_H is plotted in Fig. 12. Comparing N_H at the onset of the phase transition (N_H = 276 and 318 electrons for DLPE and DMPE, respectively) with the number expected for the head group (N_H = 140 electrons per molecule) gives a difference of 136 or 178 electrons, respectively. These extra electrons would result from a hydration of the head group region by 14, respectively, 18 water molecules per lipid. This number should be compared with the hydration number 8–10 for the fluid phase, deduced (Seddon et al., 1984; McIntosh and Simon 1986) from the x-ray long spacings of multilayers in various phases of several phosphatidyl ethanolamines. The reduction of N_H with decreasing area would then be due to water being squeezed out of the head group region on compression.

Phase coexistence range (II)

It is interesting to compare the change during the main phase transition of the parameters for the hydrocarbon moiety with that observed in bilayers. In going from the fluid to the solid phase, ρ_T/ρ_w changes from 0.89 to 0.98, i.e., by 10%. For bilayers the density changes during the phase transition have been reported to be <3% (Seddon et al., 1984) whereas for phosphatidyl cholines, too, it has been shown that not only the average molar density but also the density of the hydrocarbon moiety change by <10% (Schmidt and Knoll, 1985). This indicates that even at surface pressures as high as 25 mN/m the changes which occur during the monolayer phase transition are considerably different from those observed in the comparable phase transition in bilayers. This is probably connected to the fact that, in the monolayer, the hydrocarbon region faces the air, whereas in the bilayer it is confined by the hydrophobic moieties on both sides. In fact, for comparable surface tension, the roughness of the monolayer is larger in the fluid phase in the ordered phase. (Als-Nielsen and Möhwald, 1989). In view of this, we have tried as well to refine the two-box model by allowing a larger smearing of the hydrocarbon/gas interface than of the lower interfaces. This, however, affected ρ_T by <3% whereas the results for the hydrocarbon/gas smearing were ambiguous.

On the other hand, changes of the thickness l_T of the hydrocarbon moiety of nearly 30% have been reported by Janiak et al. (1976) for bilayers and this is close to the changes of l_T reported in this work.

In conclusion, monolayer and bilayer main phase transitions are similar with respect to layer thickness but dissimilar in terms of density. This seems to indicate that, in a bilayer, the monolayer experiences a different internal pressure from that at the air-water interface.

Fig. 11 shows a linear dependence of Q_{min} on molecular area A. For coexisting, unchanging phases, the molar fraction Φ of the solid phase, is related to the molecular areas according to

$$\Phi = (A_{fl} - A)/(A_{fl} - A_s), \quad (41)$$

while the area fraction

$$\Phi' = A_s/A \cdot \Phi = A_s/A \cdot (A_{fl} - A)/(A_{fl} - A_s), \quad (42)$$

where A, A_{fl} and A_s are the mean, fluid, and solid molecular areas, respectively (cf Kjaer et al., 1987; and Helm et al., 1987*a*). Hence, the linear dependence of Q_{min} on A corresponds to a linear dependence of Φ on A and by extrapolation to Φ = 0 and Φ = 1 one can derive the areas A_{fl} and A_s.

Studies of the phase coexistence range yield information on the coexisting ordered phase ($\Pi < \Pi_s$). The diffraction experiments (discussed in the next section) demonstrate that this phase undergoes a structural change on approaching Π_s from below. Quantitative fluorescence microscopic studies (Helm and Möhwald, 1988; Flörsheimer, 1989) demonstrate that the molecular area of the denser coexisting phase is 10–20% larger in the middle of the coexistence range than the value at Π_s.

Surface potential data (Miller et al., 1987), too, indicate the onset of a structural change of the denser coexisting phase (at an area per molecule of 50 Å^2), but the data are difficult to interpret at the molecular level.

A structural change of this phase is indicated as well by our x-ray reflectivity measurements, because the curves for the higher pressures do not go through the isosbestic point (Fig. 8 *b*). The linear dependence of Q_{min}

on mean molecular area (Fig. 11) gives a lower limit of 43 Å^2 for the area of the denser coexisting phase. For the molecular arrangement at 43 Å^2 the following three extremes may be considered: (*a*) the tails are straight and normal to the surface. This gives a value of l_T as expected for the fully condensed phase $> \Pi_s$ but an 8% lower density ρ_T; (*b*) the tails are uniformly tilted and condensed. This gives an 8% smaller thickness l_T but the same density as $> \Pi_s$; (*c*) the tails are not in the all-*trans* configuration and exhibit many defects; this would give values for both l_T and ρ_T in between the above extremes.

In fact (Fig. 10), the value obtained for ρ_T is as large as that expected for close packed chains, although the molecular area is 8% larger than the area $A = 40$ Å^2 expected for close packing. The thickness l_T is ~ 1 Å smaller than that obtained for an area $A = 40$ Å^2. These findings suggest a uniform chain tilt as was previously derived for arachidic acid monolayers on pure water (Kjaer et al., 1989) and as has sometimes been suggested on the basis of pressure vs. area isotherms (Albrecht, et al., 1978). Indeed, recent rod scan data (Möhwald et al., 1990) indicate a uniform tilt (towards next-nearest neighbour tails). Thus, model (*b*) (close-packed domains of uniform tilt) is indicated. The positional coherence length may be limited by the size of these domains. However, the positional coherence length is lower for DMPE at $\Pi < \Pi_s$ (15–20 lattice spacings at 43 Å^2) than for the tilted phase of arachidic acid (30–40 spacings). (Kjaer et al., 1989).

Transition at Π_s (II → III)

In a previous work on DMPA monolayers (Kjaer et al., 1987; Helm et al., 1987*a*) we have shown that on increase of the lateral pressure $\Pi > \Pi_s$ the translational order range ξ increases dramatically from ~ 10 spacings to nearly 100 spacings. In the present work on DMPE, we observe an increase of ξ from ~ 10 spacings well below Π_s to 50–70 spacing above Π_s. The integrated intensity, too, increases as Π_s is approached, whereas the lattice spacing d goes continuously through the transition, albeit with a change of the slope κ_d. All this is consistent with the behaviour observed for DMPA and may well be the typical behaviour for a phospholipid with a small head group. The present DMPE data, due to its smaller scatter and more densely spaced data points, allows a more detailed analysis of the transition than was possible for DMPA. The compressibility κ_d changes by more than a factor of two at the transition, whereas ρ_T is unchanged to within an accuracy of 1%. Also, the thickness l_T of the tail layer goes continuously through the transition. These findings show that the transition is of second order and, together with the observation of a finite positional correlation length on both sides of the transition and electron diffraction results (Fischer and Sackmann, 1986) which show that in films transferred onto solid, amorphous supports the angular correlations extend over several micrometers, are consistent with a transition from a hexatic phase to a hexatic glass (Nelson and Halperin, 1979; Nelson, 1983; and Nelson et al., 1982). In a future publication we hope to learn more about this transition by comparing calculated (Peterson et al., 1990) and measured diffraction line-shapes. Here, we merely state the experimental results.

Both for DMPA at high pressures (Kjaer et al., 1987; Helm et al., 1987*a*) and for DMPE, Lorentzian line shapes gave significantly better fits than did Gaussians, whereas equally good fits resulted with either line shape for DMPE at lower pressures (areas $A > \sim 42$ Å^2).

We clearly observe a reduction in head group size and an increase of ρ_H on compression, indicating that the electron rich parts of the head group are confined more strictly within one plane. This is accompanied by a reduction of N_H, suggesting a reduced hydration (cf Fig. 12 which gives N_H vs. mean molecular area A). Starting from the most expanded state, N_H decreases linearly with a slope

$$dN_H/dA = 4.0\, e/\text{Å}^2. \tag{43}$$

With $A_{lipid:H}$ denoting the molecular area solely due to the lipid and $\rho_{lipid:H}$ denoting the density due to a head group confined in that area, one expects

$$N_H = \rho_{lipid:H} \cdot A_{lipid:H} \cdot l_H + \rho_W \cdot (A - A_{lipid:H}) \cdot l_H \tag{44}$$

$$= A_{lipid:H} \cdot l_H \cdot (\rho_{lipid:H} - \rho_W) + A \cdot l_H \cdot \rho_W, \tag{45}$$

when

$$dN_H/dA = \rho W \cdot l_H = 3.7\, e/\text{Å}^2, \tag{46}$$

using $l_H \approx 11$ Å $\approx$ constant in the expanded regime. The slope, however, changes dramatically on approaching Π_s where l_H changes faster, again demonstrating the strong dehydration and head group ordering.

The solid phase ($\Pi > \Pi_s$, III)

In the most ordered phase ($\Pi > \Pi_s$) of DMPE, the positional coherence length ξ is as large as in films of DMPA or arachidic acid (Kjaer et al., 1989). As with arachidic acid (Fisher and Sackmann, 1986), electron diffraction data from DMPE monolayers on solid supports (op. cit.) clearly demonstrated a hexagonal structure. In view of these similarities, it is perhaps not surprising that the same high value of the tail density has been found here for DMPE as for arachidic acid (Kjaer et al., 1989): $\rho_T = (0.98 \pm 0.01) \cdot \rho_W$.

The thickness ($l_T = [15.5 \pm 0.5]$Å) of the hydrocarbon layer is ~ 1 Å less than the value (16.6 Å, Eq. 20)

expected for the vertical all-*trans* chain. (The Bragg rod data indicate a molecular tilt-angle $t < 5°$. And 16.6 Å · cos 5° = 16.5 Å). It is conceivable that this discrepancy is due to one of the carbonyl groups being buried into the tail region as previously discussed, or to some other shortcoming of the somewhat simplistic model description of the monolayer. (The assumption of ~1 *g-t-g*-kink per chain would also lead to a 1 Å thinner hydrocarbon layer. This mechanism can, however, be ruled out because [*a*] with the chains vertical, the kinks would disrupt the close packing, in contradiction with the high density deduced from the reflectivity data; and [*b*] further, the laterally crystalline packing would be disturbed, in contradiction with the observation of positional coherence lengths of some 50 spacings.) It is worth mentioning that this problem was encountered with arachidic acid (op. cit), too, when the data was least squares fitted by adjusting the density and thickness of the tail layer with the number of electrons, N_T, fixed at the expected value of 153 electrons: the tail thickness came out ~1 Å too small. Altogether, this suggests that the interface between tail and head sections of the model is somewhat displaced towards the tail as compared with the sketch in Fig. 3. In consequence, this would cause l_H to be enlarged. However, due to hydration, interaction with any ions present, et cetera, l_H is, anyway, more ambiguous.

If, now, we compare the number ($N_H = 155$) of electrons in the head group with the number $N_H = 140$ expected for the bare head group, the difference of a mere 1.5 water molecule suggests that the state above Π_s is that of the monohydrate.

The question, to which extent this and other conclusions based on the *XR* is affected by the details of the model used (in particular the division of the monolayer into head and tail layers), was addressed in the following way: Reflectivity curves measured in the condensed phase were also fitted, with a slab model assuming a shift of the interface between head and tail slabs (cf section on analysis of x-ray reflectivity data). This was achieved by varying N_T by up to 5%. We first noted that, in all fits, the monolayer thickness measured $l_T + \frac{1}{2}l_H$ (cf Eq. 40*a*) was constant (to within 0.4%). ρ_T, on the other hand, varied <1% while ρ_H increases slightly (<2%) with N_T. The densities being nearly constant, l_T and l_H depend almost linearly on N_T. With $l_T + \frac{1}{2}l_H \simeq$ constant, it is evident that an increase of N_T decreases N_H and vice versa. Elder et al. (1977) found that in DLPE crystals, the tails are mutually displaced orthogonal to the layers. On assuming such a configuration for the monolayer, eight electrons would be shifted to the tail slab.

At the highest pressure (when $A = A_s = 40$ Å^2; "o" in Fig. 8 and Table 1), an increase of N_T by about 5% (i.e., to 220 electrons) decreases N_H to 140. However, the whole molecule still has 10 electrons (i.e., one water molecule) more than suggested by its structure formula. On the other hand, decreasing N_T to 200 gives $N_H = 167$ electrons and a hydration of 1.7 water molecules. l_T varies between 16.4 Å and 15.2 Å.

Similarly, at the lowest pressures of the solid phase (when $A = 42.8$Å2; "j" in Fig. 8 and Table 1), increasing N_T to 220 gave $N_H = 164$, whereas $N_T = 220$ increased N_H to 194.

These numbers show that the deduced state of hydration is barely influenced by slight shifts in the model assumptions. The same is true of the tail density, whereas of course the tail layer thickness is more sensitive. Similar conclusions were reached for arachidic acid (op. cit.).

Whereas the model could thus be improved on, a refined model would involve more parameters. With the available data, no conclusive results could be obtained with more parameters. We further note that, for the two molecules studied, the proposed model gives the same results for the head group whereas the film thicknesses differ by 2–3 Å (Fig. 10, l_T, l_{Sum}) in both the fluid and the solid phases, in good agreement with the expected 2 · 1.265 Å. Finally, the results for the total thickness agree reasonably well with the results for bilayers in the L_β phase (½ · 55 Å and ½ · 50.5 Å for DMPE and DLPE, respectively) whereas the extension of the head group and its decreasing hydration on compression appear reasonable in the light of molecular models. In future experiments, combination of x-ray and neutron reflectivity measurements may further elucidate the monolayer structures (cf Vaknin et al., 1991).

CONCLUSION

This work has presented a detailed x-ray study of monolayers of DMPE and DLPE, two rather similar phospholipids: the molecules exhibit identical head groups (phosphatidylethanolamine) and indeed the structural parameters (head group extension l_H and electron density ρ_H) for the two systems do agree when comparing the same phase and mean molecular area. They differ in chain length by two CH_2 units and, indeed, the thicknesses l_T of the hydrophobic region differ by 1.5–2.8 Å whereas the electron densities ρ_T agree within 2%. These results give support to the box model used for interpreting the x-ray reflectivity data.

The two systems show distinct phase transitions from the isotropic fluid phase ("LE") to ordered states, and all the phases have been characterized. In the fluid phase, a reduction of the mean molecular area by ~30% leads to an increase of 25% in the thickness of the hydrophobic moiety, whereas the electron density ρ_T of

the hydrophobic region increases by a mere 6%. Throughout the fluid phase the thickness l_H of the head group layer is nearly constant and the change in the electron density ρ_H can be ascribed exclusively to water being squeezed out. The fact that l_H ($\sim$11Å) is considerably larger than expected from molecular models (7 ± 2 Å) may, as discussed above, be due to the two hydrocarbon tails being mutually displaced, leading to an effective increase of l_H at the expense of l_T.

In the region where the fluid phase ("LE") coexists with an ordered phase the x-ray reflectivity can be described as a superposition of the contributions of the two coexisting phases, with the area fractions of the two phases obeying a lever rule. Deviations from this rule near the high pressure end of the coexistence range are due to a structural change of the ordered phase: on compression, the molecular density increases and the (uniform) tilt angle of the aliphatic chain decreases. At sufficiently high lateral pressures the tilt angle is close to zero.

Comparing the fluid and the ordered phases, the electron densities ρ_T of the hydrophobic moiety differ by more than 10%, and this difference is larger than for the corresponding phases of bilayer membranes. The variation of the parameters l_H and ρ_H indicates that the change of the ordered phase is accompanied by dehydration and (possibly) ordering of the head groups. In DMPA, the corresponding phosphatidic acid, this transition was seen (Kjaer et al., 1987; Helm et al., 1987*a*) as a change in the positional coherence length. This effect is also observed in the present system (DMPE). Further, a discontinuity of the lateral compressibility marks the transition.

Received for publication 4 February 1991 and in final form 17 June 1991.

REFERENCES

Albrecht, O., H. Gruler, and E. Sackmann. 1978. "Polymorphism of phospholipid monolayers." *J. Physiol. (Paris).* 39:301–313.

Als-Nielsen, J. 1987. Solid and liquid surfaces studied by synchrotron x-ray diffraction. *In* Structures and Dynamics of Surfaces. Vol. 2. W. Schommers, and P. von Blanckenhagen, editors. Springer Verlag, Berlin.

Als-Nielsen, J., and H. Möhwald. 1989. Synchrotron x-ray scattering studies of langmuir films. *In* Handbook of Synchrotron Radiation, Vol. 4. S. Ebashi, E. Rubinstein, and M. Koch, editors. North Holland Publishing Co., Amsterdam.

Als-Nielsen, J., and K. Kjaer (1989). X-ray reflectivity and diffraction studies of liquid surfaces and surfactant monolayers. *In* The proceedings of the Nato Advanced Study Institute, Phase Transitions in Soft Condensed Matter, Geilo, Norway, April 4–April 14, 1989. T. Riste and D. Sherrington, editors. Plenum Publishing Corp., NY.

Bareman, J. P., G. Cardini, and M. Klein. 1988. Characterization of structural and dynamical behavior of long-chain molecules using molecular-dynamics calculations. *Phys. Rev. Lett.* 60:2152–2155.

Braslau, A., M. Deutsch, P. S. Pershan, A. H. Weiss, J. Als-Nielsen, and J. Bohr. 1985. Surface Roughness of Water Measured by X-ray Reflectivity. *Phys. Rev. Lett.* 54:114–117.

Braslau, A., P. S. Pershan, G. Swislow, B. M. Ocko, J. Als-Nielsen. 1988. Capillary waves on the surface of simple liquids measured by x-ray reflectivity. *Phys. Rev.* A38:2457–2470.

Daillant, J., L. Bosio, J. J. Benattar, and J. Meunier. 1989. Capillary waves and bending elasticity of monolayers on water studied by x-ray reflectivity as a function of surface pressure. *Europhys. Lett.* 8:453–458.

Elder, M., P. Hitchcock, R. Mason, and G. G. Shipley. 1977. A refinement analysis of the crystallography of the phospholipid, 1,2-dilauroyl-DL-phosphatidylethanolamine, and some remarks on lipid–lipid and lipid–protein interactions." *Proc. R. Soc. Lond. A Math. Phys. Sci.* 354:157–170.

Fischer, A., and E. Sackmann. 1986. Electron microscopy and electron diffraction study of coexisting phases of pure and mixed monolayers transferred onto solid substrates. *J. Colloid Sci.* 112:1–14.

Flörsheimer, M. 1989. Licht- und elektronenoptische, elektrische und thermodynamische Untersuchungen zur mikroskopischen Struktur sowie zur Keimbildung in ultradünnen Filmen. Ph.D. thesis. Technische Universität, Munich. 186 pp.

Flörsheimer, M., and H. Möhwald. 1991. Superimposed ordering transitions in phospolid monolayers. *Colloids and Surfaces.* In press.

Gaines, G. 1966. Insoluble monolayers at liquid-gas interfaces. Interscience, New York. 386 pp.

Helm, C. A., and H. Möhwald. 1988. Equilibrium and nonequilibrium features determining superlattices in phospholipid monolayers. *J. Phys. Chem.* 82:1262–1266.

Helm, C. A., H. Möhwald, K. Kjaer, and J. Als-Nielsen. 1987*a*. Phospholipid monolayers between fluid and solid states. *Biophys. J.* 52:381–390.

Helm, C. A., H. Möhwald, K. Kjaer, and J. Als-Nielsen. 1987*b*. Phospholipid monolayer density distribution perpendicular to the water surface. A synchrotron x-ray reflectivity study. *Europhys. Lett.* 4:697–703.

Jacquemain, D., S. Grayer Wolf, F. Leveiller, M. Lahav, L. Leiserowitz, M. Deutsch, K. Kjaer, and J. Als-Nielsen. 1989. Crystalline self-aggregation and a pressure driven solid–solid phase transition in a fluorinated Langmuir monolayer. *Colloque de Physique (Paris).* 50:29–37.

Jacquemain, D., S. Grayer Wolf, F. Leveiller, M. Lahav, L. Leiserowitz, M. Deutsch, K. Kjaer, and J. Als-Nielsen. 1990. Dynamics of two-dimensional self-aggregation, pressure and pH induced structural changes in a fluorinated amphiphile at liquid-air interfaces. An x-ray synchrotron study. *J. Am. Chem. Soc.* 112:7724–7736.

Janiak, M. J., D. M. Small, and G. G. Shipley. 1976. Nature of the thermal pretransition of synthetic phospholipids: dimyristoyl- and dipalmitoyllecithin. *Biochemistry.* 15:4575–4580.

Kenn, R.M., C. Böhm, A. M. Bibo, I. R. Peterson, H. Möhwald, J. Als-Nielsen, and K. Kjaer. 1991. Mesophases and crystalline phases in fatty acid monolayers. *J. Phys. Chem.* 95:2092–2097.

Kjaer, K., J. Als-Nielsen, C. A. Helm, L. A. Laxhuber, and H. Möhwald. 1987. Ordering in lipid monolayers studied by synchrotron x-ray diffraction and fluorescence microscopy. *Phys. Rev. Lett.* 58:2224–2227.

Kjaer, K., J. Als-Nielsen, C. A. Helm, P. Tippman-Krayer, and H. Möhwald. 1989. Synchrotron x-ray diffraction and reflection studies

of arachidic acid monolayers at the air-water interface. *J. Phys. Chem.* 93:3200–3206.

Leveiller F., D. Jacquemain, M. Lahav, L. Leiserowitz, M. Deutsch, K. Kjaer, and J. Als-Nielsen. 1991. Crystallinity of the double layer of cadmium arachidate films at the water surface. *Science (Wash. DC).* 252:1532–1356.

Lösche, M. 1986. Das Phasenverhalten eines Quasi-Zweidimensionalen Dielektrikums an der Elecktrolyt/Gas-Grenzfläche. Ph.D. thesis. Technical University of Munich, Germany. 210 p.p.

Lösche, M., J. Rabe, A. Fischer, B. U. Rucha, W. Knoll, and H. Möhwald. 1984. Microscopically observed preparation of Langmuir-Blodgett films. *Thin Solid Films.* 117:269–280.

McIntosh, T. J., and S. A. Simon. 1986. Area per molecule and distribution of water in fully hydrated dilauroylphosphatidylethanolamine bilayers. *Biochemistry.* 25:4948–4952. (Erratum, 25:8474.)

Miller, A., C. A. Helm, and H. Möhwald. 1987. The colloidal nature of phospholipid monolayers. *J. Physique. (Paris).* 48:693–701.

Möhwald, H., R. M. Kenn, D. Degenhardt, K. Kjaer, and J. Als-Nielsen. 1990. Partial order in phospholid monolayers. *Physica A.* 168:127–139.

Nelson, D. R., and B. J. Halperin. 1979. Dislocation-mediated melting in two dimensions. *Phys. Rev. B.* 19:2457–2484.

Nelson, D. R., M. Rubinstein, and F. Spaepen. 1982. Order in two-dimensional binary random arrays. *Phil. Mag. A.* Taylor and Francis, London. 46:105–126.

Nelson, D. R. 1983. Reetrant melting in solid films with quenched random impurities. *Phys. Rev. B.* 27:2902–2914.

Peterson, I. R., R. Steitz, H. Krug, and G. Voigt-Martin. 1990. An investigation of the spot profiles in transmission electron diffraction from Langmuir-Blodgett films of aliphatic chain compounds. *J. Physique (Paris).* 51:1003–1026.

Schmidt, G., and W. Knoll. 1985. Densitometric characterization of aqueous lipid dispersions. *Ber. Bunsenges. Phys. Chem.* 89:36–43.

Seddon, J. M., G. Cevc, R. D. Kaye, and D. Marsh. 1984. X-ray diffraction study of the polymorphism of hydrated diacyl- and dialkylphosphatidylethanolamines. *Biochemistry.* 23:2364–2644.

Vaknin, D., K. Kjaer, J. Als-Nielsen, and M. Lösche. 1991. Structural properties of phosphatidylcholine in a monolayer at the air/water interface. Neutron reflection study and reexamination of x-ray reflection measurements. *Biophys. J.* 59:1325–1332.

Vineyard, G. 1982. Grazing-incidence diffraction and the distorted-wave approximation for the study of surfaces. *Phys. Rev. B.* 26:4146–4159.

Wolf, S. G., M. Deutsch, E. M. Landau, M. Lahav, L. Leiserowitz, K. Kjaer, and J. Als-Nielsen. 1988. A synchrotron x-ray study of a solid–solid phase transition in a two-dimensional crystal. *Science (Wash. DC).* 242:1286–1290.